Available online at www.sciencedirect.com
SCIENCE DIRECT®
International Journal of Mass Spectrometry 227 (2003) 339–360
International Journal of Mass Spectrometry
www.elsevier.com/locate/ijms

Influence of substituents on cation-π interactions. 3. Absolute binding energies of alkali metal cation−aniline complexes determined by threshold collision-induced dissociation and theoretical studies

R. Amunugama, M.T. Rodgers*

Department of Chemistry, Wayne State University, Detroit, MI 48202, USA

Received 23 February 2002; accepted 22 May 2002

Abstract

Threshold collision-induced dissociation of $M^+(C_6H_5NH_2)_x$ with Xe is studied using guided ion beam mass spectrometry. M^+ include the following alkali metal ions: Li^+, Na^+, K^+, Rb^+, and Cs^+. Both mono- and bis-complexes are examined (i.e., $x = 1$ and 2). In all cases, the primary and lowest energy dissociation channel observed is endothermic loss of an intact aniline ligand. Sequential dissociation of a second aniline ligand is observed at elevated energies in the bis-complexes. Minor production of ligand exchange products, M^+Xe and $M^+(C_6H_5NH_2)Xe$, is also observed. The cross-section thresholds for the primary dissociation channel are interpreted to yield 0 and 298 K bond dissociation energies (BDEs) for $(C_6H_5NH_2)_{x-1}M^+$–$C_6H_5NH_2$, $x = 1$ and 2, after accounting for the effects of multiple ion–neutral collisions, the kinetic and internal energies of the reactants, and dissociation lifetimes. Density functional theory calculations at the B3LYP/6-31G* level of theory are used to determine the structures of these complexes and provide molecular constants necessary for the thermodynamic analysis of the experimental data. Theoretical binding energies are determined from single point calculations at the MP2(full)/6-311+G(2d,2p) level using the B3LYP/6-31G* geometries. Zero point energy and basis set superposition error corrections are also included. The agreement between theory and experiment is very good in all cases except for the $Li^+(C_6H_4NH_2)$ complex where theory underestimated the binding in this complex. The trends in $M^+(C_6H_5NH_2)_x$ binding energies are explained in terms of varying magnitudes of electrostatic interactions and ligand–ligand repulsion in the complexes. Comparisons are also made to previously determined experimental BDEs of $M^+(C_6H_6)_x$, $M^+(C_6H_5CH_3)_x$, and $M^+(C_6H_5F)_x$ to examine the influence of the substituent on the binding, and the factors that control the strength of cation-π interactions.

Keywords: Alkali metal ions; Bond dissociation energies; Cation-π interactions; Collision-induced dissociation; Guided ion beams

1. Introduction

The cation-π interaction has become a fascinating topic among chemists, biophysicists, and biologists. The number of publications related to the study of cation-π interactions has grown significantly over the

* Corresponding author. Tel.: +1-313-577-2431; fax: +1-313-577-8822.
E-mail address: mrodgers@chem.wayne.edu (M.T. Rodgers).

1387-3806/03/$ – see front matter © 2003 Elsevier Science B.V. All rights reserved.
doi:10.1016/S1387-3806(03)00104-0

last decade. Amongst the recent investigations aimed at achieving a better understanding of this important biochemical interaction are a variety of experimental [1–12] and quantum-chemical studies [13–18], as well as comprehensive review articles [6,19,20]. These studies highlight both the fundamental nature of cation-π interactions and their role in biological systems. Although the cation-π interaction has only recently come to be appreciated as an important noncovalent binding force, this interaction is not new to experimentalists. It has been over 20 years since Kebarle and coworkers showed that the enthalpic interaction of K^+ with benzene, a cation-π interaction, was quite strong. Indeed, the measured binding energy of K^+ to benzene was found to be stronger than that between K^+ and H_2O. This early result was quite surprising because a strong interaction of a cation with a neutral molecule was generally believed to result from an ion–dipole interaction. Therefore, benzene, a nonpolar molecule with no permanent dipole, was not expected to bind to a cation more strongly than water, a highly polar molecule with a substantial dipole moment [21]. In biological systems, such as proteins, this interaction exists between a positively charged species, such as a metal ion or a protonated side chain of a basic amino acid (e.g., lysine or arginine), and an aromatic π face. A great deal of attention has been focused on cation-π interactions involving the alkali metal cations, and in particular, Na^+ and K^+, the most biologically relevant alkali metal cations [22]. Such alkali metal cation-π interactions are recognized as strong noncovalent binding forces that play an important role in a wide variety of fields ranging from materials design [23] to molecular biology. Recent observations have led to a constantly expanding appreciation of the involvement of cation-π interactions in protein structural organization [19,20,24–28], the functioning of ionic channels in membranes [29,30], and the role that these interactions might play in molecular recognition [31]. Thus, it is of paramount importance to understand cation-π interactions both from a fundamental perspective as well as the detailed role that they play in biological systems.

Studies of alkali metal cations binding to model aromatic systems can be used to gain a better understanding of the interaction of these cations with large biological molecules. Furthermore, characterizing these interactions in the gas phase is an important and essential part of building a database of information concerning the nature and strength of cation-π interactions and the influence of the local environment on such interactions. A number of model systems [1,2,8–12,21,32–34], as well as the aromatic amino acids [3,4] in which the neutral ligand binds to the metal ion through its π electrons, have been studied in the gas phase. Among the model systems, benzene [8,9,21,32–34] and pyrrole [2,10], and their derivatives, such as phenol and indole [1], toluene [11], and fluorobenzene [12], are of particular interest because they constitute the simplest groups of larger aromatic ligands that could mimic the binding properties of complex π ligands that might participate in cation-π interactions operative in biological systems. High-level theoretical calculations have also been performed for several of the earlier described systems [1,2,10,17–19] and several substituted benzenes, including aniline [14], at various levels of theory. In fact, of the alkali metal ions, cation-π interactions to aniline were only calculated for binding to Na^+. Previous experimental investigations of cation-π interactions between metal ions and aniline have been limited to the Cr^+, Fe^+, and Co^+ cations [7].

In recent work, we have developed methods to allow the application of quantitative threshold collision-induced dissociation (CID) methods to obtain accurate thermodynamic information on an increasingly large body of model organic and biological systems [8–12,35–49]. One of the driving forces behind these developments is our interest in applying such techniques to systems having biological relevance. In addition, we seek to perform accurate thermochemical measurements that provide absolute anchors for metal cation affinity scales over an ever-broadening range of energies and molecular systems. In the present paper, we examine cation-π interactions of aniline, $C_6H_5NH_2$, with the alkali metal ions, Li^+, Na^+, K^+, Rb^+, and Cs^+. The structure of aniline along with its measured [50] and calculated dipole moments (determined here) and estimated polarizability [51]

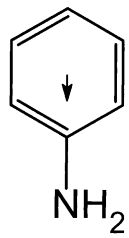

Fig. 1. Structure of the aniline molecule. The properly scaled dipole moment in Debye is shown as an arrow. It should be noted that the dipole moment is actually oriented out of the plane of the aromatic ring at an angle of ∼45°. Values listed are taken from experiment [50] and theoretical calculations performed here (in parentheses). The estimated polarizability is also shown [51].

are shown in Fig. 1. The kinetic energy-dependent cross-sections for the CID processes are analyzed using methods developed previously [39]. The analysis explicitly includes the effects of the internal and translational energy distributions of the reactants, multiple ion–neutral collisions, and the lifetime for dissociation. We derive $(C_6H_5NH_2)_{x-1}M^+$–$C_6H_5NH_2$, $x = 1$ and 2, bond dissociation energies (BDEs) for all of the complexes and compare these results to ab initio and density functional calculations performed here and in the literature [14]. Comparisons are also made to the analogous benzene [9], toluene [11], and fluorobenzene [12] systems studied previously to examine the influence of the amine substituent on the binding, and the factors that control the strength of cation-π interactions. Comparison is also made to previous measurements of cation-π interactions between transition metal ions and aniline [7].

2. Experimental section

2.1. General procedures

Cross-sections for CID of $M^+(C_6H_5NH_2)_x$ complexes, where $x = 1$ and 2, and $M^+ = Li^+$, Na^+, K^+, Rb^+, and Cs^+, are measured using a guided ion beam mass spectrometer that has been described in detail previously [44]. The $M^+(C_6H_5NH_2)_x$ complexes are generated in a flow tube ion source by condensation of the alkali metal ion and neutral aniline molecule(s). These complexes are collisionally stabilized and thermalized by ∼10^5 collisions with the He and Ar bath gases such that the internal energies of the ions emanating from the source region are well described by a Maxwell–Boltzmann distribution at room temperature [44]. The ions are extracted from the source, accelerated, and focused into a magnetic sector momentum analyzer for mass analysis. Mass-selected ions are decelerated to a desired kinetic energy and focused into an octopole ion guide, which traps the ions in the radial direction [52]. The octopole passes through a static gas cell containing Xe, used as the collision gas, for reasons described elsewhere [53–55]. Low gas pressures in the cell (typically 0.05–0.20 mTorr) are used to ensure that multiple ion–neutral collisions are improbable. Product and unreacted beam ions drift to the end of the octopole where they are focused into a quadrupole mass filter for mass analysis and subsequently detected with a secondary electron scintillation detector and standard pulse counting techniques.

Ion intensities are converted to absolute cross-sections as described previously [56]. Absolute uncertainties in cross-section magnitudes are estimated to be ±20%, which are largely the result of errors in the pressure measurement and the length of the interaction region. Relative uncertainties are approximately ±5%. Because the radio frequency used for the octopole does not trap light masses with high efficiency, absolute magnitudes of the cross-sections for production of Li^+ are probably accurate to ±50%.

Ion kinetic energies in the laboratory frame, E_{lab}, are converted to energies in the center-of-mass (CM) frame, E_{CM}, using the formula $E_{CM} = E_{lab}m/(m+M)$, where M and m are the masses of the ionic and neutral reactants, respectively. All energies reported below are in the CM frame unless otherwise noted. The absolute zero and distribution of the ion kinetic energies are determined using the octopole ion guide as a retarding potential analyzer as previously described [56]. The distribution of ion kinetic

energies is Gaussian with an fwhm between 0.2 and 0.4 eV (lab) for these experiments. The uncertainty in the absolute energy scale is ±0.05 eV (lab).

Because multiple collisions can influence the shape of CID cross-sections and the threshold regions are most sensitive to these effects, we have performed pressure-dependent studies of all cross-sections examined here. In the present systems, we observe small cross-sections at low energies that have an obvious dependence upon pressure. We attribute this to multiple energizing collisions that lead to an enhanced probability of dissociation below threshold as a result of the longer residence time of these slower moving ions. Data free from pressure effects are obtained by extrapolating to zero reactant pressure, as described previously [57]. Thus, results reported below are due to single bimolecular encounters.

2.2. Thermochemical analysis

The threshold regions of the reaction cross-sections are modeled using Eq. (1),

$$\sigma(E) = \sigma_0 \sum_i g_i (E + E_i - E_0)^n / E \quad (1)$$

where σ_0 is an energy-independent scaling factor, E is the relative translational energy of the reactants, E_0 is the threshold for reaction of the ground electronic and ro-vibrational state, and n is an adjustable parameter. The summation is over the ro-vibrational states of the reactant ions, i, where E_i is the excitation energy of each ro-vibrational state, and g_i is the population of those states ($\sum g_i = 1$). The populations of excited ro-vibrational levels are not negligible even at 298 K as a result of the many low-frequency modes present in these ions. The relative reactivity of all ro-vibrational states, as reflected by σ_0 and n, is assumed to be equivalent.

The Beyer–Swinehart algorithm [58] is used to evaluate the density of the ro-vibrational states, and the relative populations, g_i, are calculated by an appropriate Maxwell–Boltzmann distribution at the 298 K temperature appropriated for the reactants. The vibrational frequencies of the reactant complexes are determined from density functional theory calculations as discussed in Section 2.3. The average vibrational energies at 298 K of the $M^+(C_6H_5NH_2)_x$ complexes are given in Table 1. We have estimated the sensitivity of our analysis to the deviations from the true frequencies by increasing and decreasing the scaled calculated frequencies by 10% to encompass the range of average scaling factors needed to bring calculated frequencies into agreement with experimentally determined frequencies as found by Pople et al. [59]. For the $M^+(C_6H_5NH_2)_x$ complexes with $M^+ = Rb^+$ and Cs^+, 20% variations were applied. The corresponding change in the average vibrational energy is taken to be an estimate of one standard deviation of the uncertainty in vibrational energy and varies from 0.02 to 0.07 eV for the $M^+(C_6H_5NH_2)_x$ complexes examined here (Table 1).

We also consider the possibility that collisionally activated complex ions do not dissociate on the time scale of our experiment ($\sim 10^{-4}$ s) by including statistical theories for unimolecular dissociation, specifically Rice–Ramsperger–Kassel–Marcus (RRKM) theory, into Eq. (1) as described in detail elsewhere [39,60]. The ro-vibrational frequencies appropriate for the energized molecules and the transition states (TSs) leading to dissociation are given in Tables 1 and 2. In our analysis, we assume that the TSs are loose and product-like because the interaction between the alkali metal ion and the aniline ligand(s) is largely electrostatic (ion–quadrupole, ion–dipole, and ion-induced dipole interactions). Thus, the most appropriate model for the TS is a loose phase space limit (PSL) model located at the centrifugal barrier for the interaction of $M^+(C_6H_5NH_2)_{x-1}$ with $C_6H_5NH_2$ as described in detail elsewhere [39]. The TS vibrations appropriate for this model are the frequencies of the products, which are also found in Table 1. The transitional frequencies, those that become rotations of the completely dissociated products, are treated as rotors. Two of these transitional mode rotors have rotational constants equal to those of the neutral $C_6H_5NH_2$ product with axes perpendicular to the reaction coordinate, and correspond to its two-dimensional (2-D) rotational constant (0.071 cm^{-1}). These are the only

Table 1
Vibrational frequencies and average vibrational energies at 298 K[a]

Species	E_{vib} (eV)[b]	Frequencies (cm^{-1})
$C_6H_5NH_2$	0.07 (0.01)	220, 280, 376, 410, 499, 526, 622, 623, 691, 749, 811, 819, 861, 929, 956, 992, 1037, 1059, 1128, 1167, 1188, 1291, 1342, 1351, 1490, 1522, 1615, 1636, 1662, 3108, 3109, 3125, 3130, 3148, 3475, 3571
$Li^+(C_6H_5NH_2)$	0.16 (0.02)	174, 258, 275, 381, 389, 415, 425, 429, 522, 528, 620, 691, 787, 822, 859, 891, 983, 984, 995, 1023, 1027, 1112, 1171, 1191, 1328, 1343, 1349, 1471, 1513, 1566, 1611, 1665, 3141, 3142, 3155, 3158, 3174, 3517, 3618
$Na^+(C_6H_5NH_2)$	0.18 (0.02)	87, 125, 209, 224, 379, 390, 418, 516, 525, 539, 620, 697, 777, 819, 847, 883, 968, 978, 991, 1024, 1038, 1117, 1169, 1190, 1322, 1325, 1350, 1475, 1511, 1579, 1616, 1666, 3130, 3131, 3145, 3148, 3165, 3500, 3597
$K^+(C_6H_5NH_2)$	0.19 (0.02)	56, 106, 143, 225, 369, 383, 415, 514, 526, 620, 624, 695, 772, 818, 840, 881, 964, 976, 991, 1028, 1048, 1123, 1169, 1189, 1307, 1332, 1351, 1480, 1513, 1591, 1622, 1667, 3123, 3124, 3140, 3143, 3161, 3484, 3577
$Rb^+(C_6H_5NH_2)$	0.19 (0.03)	48, 91, 123, 225, 369, 383, 415, 514, 526, 620, 624, 695, 772, 818, 840, 881, 964, 976, 991, 1028, 1048, 1123, 1169, 1189, 1307, 1332, 1351, 1480, 1513, 1591, 1622, 1667, 3123, 3124, 3140, 3143, 3161, 3484, 3577
$Cs^+(C_6H_5NH_2)$	0.19 (0.03)	46, 87, 117, 225, 369, 383, 415, 514, 526, 620, 624, 695, 772, 818, 840, 881, 964, 976, 991, 1028, 1048, 1123, 1169, 1189, 1307, 1332, 1351, 1480, 1513, 1591, 1622, 1667, 3123, 3124, 3140, 3143, 3161, 3484, 3577
$Li^+(C_6H_5NH_2)_2$	0.38 (0.03)	16, 41, 51, 62, 78, 111, 186, 199, 220, 232, 377, 378, 385(2), 388, 413, 414, 480, 497, 519, 521, 528, 529, 620, 621, 693(2), 775, 777, 821, 822, 845, 852, 884, 888, 970, 973, 979, 980, 991, 992, 1027, 1028, 1039, 1040, 1118(2), 1169, 1170, 1190, 1191, 1325, 1326, 1331, 1333, 1350(2), 1476, 1478, 1514, 1516, 1582, 1583, 1619(2), 1665, 1665, 3135(3), 3136, 3150(2), 3152, 3153, 3171(2), 3507(2), 3605, 3606
$Na^+(C_6H_5NH_2)_2$	0.40 (0.03)	11, 24, 32, 48, 83, 92, 97, 125, 221, 223, 238, 368(2), 380(2), 416, 417, 513, 514, 525, 526, 550, 556, 621(2), 697(2), 771, 773, 819(2), 838, 842, 880, 882, 963, 964, 977(2), 991(2), 1027(2), 1043, 1044, 1120(2), 1168(2), 1189(2), 1316(2), 1330(2), 1350(2), 1478(2), 1513, 1514, 1586, 1587, 1619, 1620, 1666(2), 3127(2), 3128(2), 3142(2), 3146(2), 3163(2), 3497(2), 3594(2)
$K^+(C_6H_5NH_2)_2$	0.40 (0.03)	4, 9, 13, 42, 59, 76, 89, 108, 162, 224, 226, 357(2), 380(2), 414, 415, 512, 513, 526(2), 618, 621(2), 624, 693, 694, 766, 768, 818(2), 834, 836, 878, 879, 959(2), 974(2), 990, 991, 1029(2), 1050(2), 1124(2), 1168(2), 1188, 1189, 1304(2), 1334(2), 1351(2), 1481(2), 1514(2), 1594(2), 1623(2), 1666(2), 3122(3), 3123, 3139(2), 3143(2), 3160(2), 3484(2), 3578(2)
$Rb^+(C_6H_5NH_2)_2$	0.41 (0.07)	3, 8, 11, 42, 51, 76, 89, 108, 139, 224, 226, 357(2), 380(2), 414, 415, 512, 513, 526(2), 618, 621(2), 624, 693, 694, 766, 768, 818(2), 834, 836, 878, 879, 959(2), 974(2), 990, 991, 1029(2), 1050(2), 1124(2), 1168(2), 1188, 1189, 1304(2), 1334(2), 1351(2), 1481(2), 1514(2), 1594(2), 1623(2), 1666(2), 3122(3), 3123, 3139(2), 3143(2), 3160(2), 3484(2), 3578(2)
$Cs^+(C_6H_5NH_2)_2$	0.41 (0.07)	3, 7, 11, 42, 48, 76, 89, 108, 133, 224, 226, 357(2), 380(2), 414, 415, 512, 513, 526(2), 618, 621(2), 624, 693, 694, 766, 768, 818(2), 834, 836, 878, 879, 959(2), 974(2), 990, 991, 1029(2), 1050(2), 1124(2), 1168(2), 1188, 1189, 1304(2), 1334(2), 1351(2), 1481(2), 1514(2), 1594(2), 1623(2), 1666(2), 3122(3), 3123, 3139(2), 3143(2), 3160(2), 3484(2), 3578(2)

[a] Vibrational frequencies are obtained from a vibrational analysis of the B3LYP/6-31G* geometry-optimized structures for these species and scaled by 0.9804. For $M^+ = Rb^+$ and Cs^+, vibrational frequencies were estimated by scaling the calculated frequencies for the analogous $K^+(C_6H_5NH_2)_x$ complexes as described in the text.
[b] Uncertainties listed in parentheses are determined as described in the text.

two transitional modes for the $M^+(C_6H_5NH_2)$ systems because these systems yield one atomic product. For $M^+(C_6H_5NH_2)_2$ complexes, three additional transitional modes exist. Two of these rotors are the rotational constants of the $M^+(C_6H_5NH_2)$ product with axes perpendicular to the reaction coordinate. Of the two rotational constants of the products with axes lying along the reaction coordinate, one is a transitional mode and is assigned as the remaining rotational constant of the $C_6H_5NH_2$ product (0.187 cm^{-1}). The other becomes the one-dimesional (1-D) external rotor of the TS. These are listed in Table 2. The 2-D

Table 2
Rotational constants of $M^+(C_6H_5NH_2)_x$ in cm^{-1}

Reactant	Energized molecule		Transition state		
	1-D[a]	2-D[b]	1-D[c]	2-D[c]	2-D[d]
$Li^+(C_6H_5NH_2)$	0.149	0.067	0.187	0.071	0.0336
$Na^+(C_6H_5NH_2)$	0.090	0.056	0.187	0.071	0.0034
$K^+(C_6H_5NH_2)$	0.063	0.045	0.187	0.071	0.0015
$Rb^+(C_6H_5NH_2)$	0.063	0.045	0.187	0.071	0.0007
$Cs^+(C_6H_5NH_2)$	0.063	0.045	0.187	0.071	0.0004
$Li^+(C_6H_5NH_2)_2$	0.033	0.014	0.149, 0.187	0.067, 0.071	0.0013
$Na^+(C_6H_5NH_2)_2$	0.031	0.011	0.090, 0.187	0.056, 0.071	0.0012
$K^+(C_6H_5NH_2)_2$	0.030	0.009	0.063, 0.187	0.045, 0.071	0.0012
$Rb^+(C_6H_5NH_2)_2$	0.030	0.009	0.063, 0.187	0.045, 0.071	0.0009
$Cs^+(C_6H_5NH_2)_2$	0.030	0.009	0.063, 0.187	0.045, 0.071	0.0007

[a] Active external.
[b] Inactive external.
[c] Rotational constants of the transition state treated as free internal rotors.
[d] 2-D rotational constant of the transition state at threshold, treated variationally and statistically.

external rotational constants of the TS are determined by assuming that the TS occurs at the centrifugal barrier for interaction of $M^+(C_6H_5NH_2)_{x-1}$ with the neutral $C_6H_5NH_2$ molecule, treated variationally as outlined elsewhere [39]. The 2-D external rotations are treated adiabatically with centrifugal effects included, consistent with the discussion of Waage and Rabinovitch [61]. In the present work, the adiabatic 2-D rotational energy is treated using a statistical distribution with explicit summation over the possible values of the rotational quantum number, as described in detail elsewhere [39].

The model represented by Eq. (1) is expected to be appropriate for translationally driven reactions [62] and has been found to reproduce CID cross-sections well in a number of previous studies [53,57,63–65]. The model is convoluted with the kinetic energy distributions of both reactants, and a nonlinear least-squares analysis of the data is performed to give optimized values for the parameters σ_0, E_0, and n. The error associated with the measurement of E_0 is estimated from the range of threshold values determined for different zero-pressure extrapolated data sets, variations associated with uncertainties in the vibrational frequencies, and the error in the absolute energy scale, 0.05 eV (lab). For analyses that include the RRKM lifetime analysis, the uncertainties in the reported E_0 values also include the effects of increasing and decreasing the time assumed available for dissociation ($\sim 10^{-4}$ s) by a factor of 2.

Eq. (1) explicitly includes the internal energy of the ion, E_i. All energy available is treated statistically because the internal (rotational and vibrational) energy of the reactants is redistributed throughout the ion upon impact with the collision gas. The threshold for dissociation is by definition the minimum energy required for dissociation, and thus corresponds to formation of products with no internal excitation. The threshold energies for dissociation reactions determined by analysis with Eq. (1) are converted to 0 K bond energies by assuming that E_0 represents the energy difference between reactants and products at 0 K.[1] This assumption requires that there are no activation barriers in excess of the endothermicity of dissociation, which should certainly be valid for the noncovalent bond fission reactions examined here [66].

2.3. Theoretical calculations

To obtain model structures, vibrational frequencies, rotational constants, and energetics for the neutral $C_6H_5NH_2$ ligand and for the $M^+(C_6H_5NH_2)_x$ complexes, ab initio and density functional theory calcula-

[1] See, for example, Fig. 1 in Dalleska et al. [53].

tions were performed using Gaussian 98 [67]. Geometry optimizations were performed at B3LYP/6-31G* level [68,69] for the $M^+(C_6H_5NH_2)_x$ complexes, where $M^+ = Li^+$, Na^+, and K^+. For complexes containing Rb^+ and Cs^+, geometry optimizations were performed using a hybrid basis set in which the effective core potentials (ECPs) and valence basis sets of Hay and Wadt were used to describe the metal ion [70], while 6-31G* basis sets were used for C and H atoms. As suggested by Glendening et al. [71], a single polarization (*d*) function was added to the Hay–Wadt valence basis set for Rb and Cs, with exponents of 0.24 and 0.19, respectively.

Vibrational analyses of the geometry-optimized structures were performed to determine the vibrational frequencies for the neutral $C_6H_5NH_2$ ligand and the $M^+(C_6H_5NH_2)_x$ complexes for $M^+ = Li^+$, Na^+, and K^+. The vibrational frequencies for the complexes to Rb^+ and Cs^+ were estimated by scaling the calculated frequencies for the analogous K^+ complexes using a procedure described in detail previously [72]. When used to model data or calculate thermal energy corrections, the calculated vibrational frequencies were scaled by a factor of 0.9804 [73]. The vibrational frequencies and rotational constants of neutral $C_6H_5NH_2$ and all $M^+(C_6H_5NH_2)_x$ complexes are listed in Tables 1 and 2, respectively. Single point energy calculations were performed at the MP2(full)/6-311+G(2d,2p) level using the B3LYP/6-31G* and B3LYP/Hybrid(6-31G*, Hay–Wadt) optimized geometries. To obtain accurate BDEs, zero point energy (ZPE) corrections were applied and basis set superposition errors (BSSEs) were subtracted from the computed dissociation energies in the full counterpoise correction [74,75]. The ZPE corrections are small and decrease with increasing size of the alkali metal ion, and are 7.1, 4.1, 3.4, 2.9, and 2.8 kJ mol^{-1} for the $M^+(C_6H_5NH_2)$ complexes and 2.9, 3.1, 2.6, 2.8, and 2.4 kJ mol^{-1} for the $M^+(C_6H_5NH_2)_2$ complexes, where $M^+ = Li^+$, Na^+, K^+, Rb^+, and Cs^+, respectively. The BSSE corrections are somewhat larger, and are 10.3, 10.5, 6.0, 7.2, and 7.1 kJ mol^{-1} for the $M^+(C_6H_5NH_2)$ complexes and 21.5, 16.1, 10.6, 11.8, and 9.0 kJ mol^{-1} for the $M^+(C_6H_5NH_2)_2$ complexes, respectively. Calculations in which M^+ interacts with the amino group were also performed for the $M^+(C_6H_5NH_2)$ complexes. In these complexes, the ZPE corrections are somewhat larger than for the ground state complexes, and are 8.0, 5.1, 4.1, 3.7, and 3.3 kJ mol^{-1}, respectively. In contrast, the BSSE corrections for these complexes are slightly smaller than for the ground state complexes and are 7.5, 8.7, 5.6, 7.2, and 6.8 kJ mol^{-1}, respectively.

3. Results

3.1. Cross-sections for CID

Experimental cross-sections were obtained for the interaction of Xe with 10 $M^+(C_6H_5NH_2)_x$ complexes, where $M^+ = Li^+$, Na^+, K^+, Rb^+, and Cs^+, and $x = 1$ and 2. Fig. 2 shows data for the $Na^+(C_6H_5NH_2)_x$, $x = 1$ and 2 complexes. The other $M^+(C_6H_5NH_2)_x$ complexes show similar behavior to that observed for the $Na^+(C_6H_5NH_2)_x$ complexes. The sequential loss of intact aniline molecules and ligand exchange with Xe are the only processes observed in these systems over the collision energy range studied, typically 0 to >5 eV. The dominant process observed for all of these complexes is the loss of a single intact aniline molecule in the CID reactions 2.

$$M^+(C_6H_5NH_2)_x + Xe \rightarrow M^+(C_6H_5NH_2)_{x-1} + C_6H_5NH_2 + Xe \quad (2)$$

The maximum cross-section for reaction 2, as well as the total cross-section, roughly doubles in magnitude from the mono- to the bis-complexes. The threshold for reaction 2 also decreases from the mono- to bis-complexes, consistent with conventional ideas of ligation of gas-phase ions, i.e., stepwise sequential bond energies decrease because of increasing electrostatic repulsion between the ligands, causing the distance between the cation and ligands to increase. Such ideas have been noted in previous experimental and theoretical studies of $M^+(ligand)_n$ clusters [48,49,76–79].

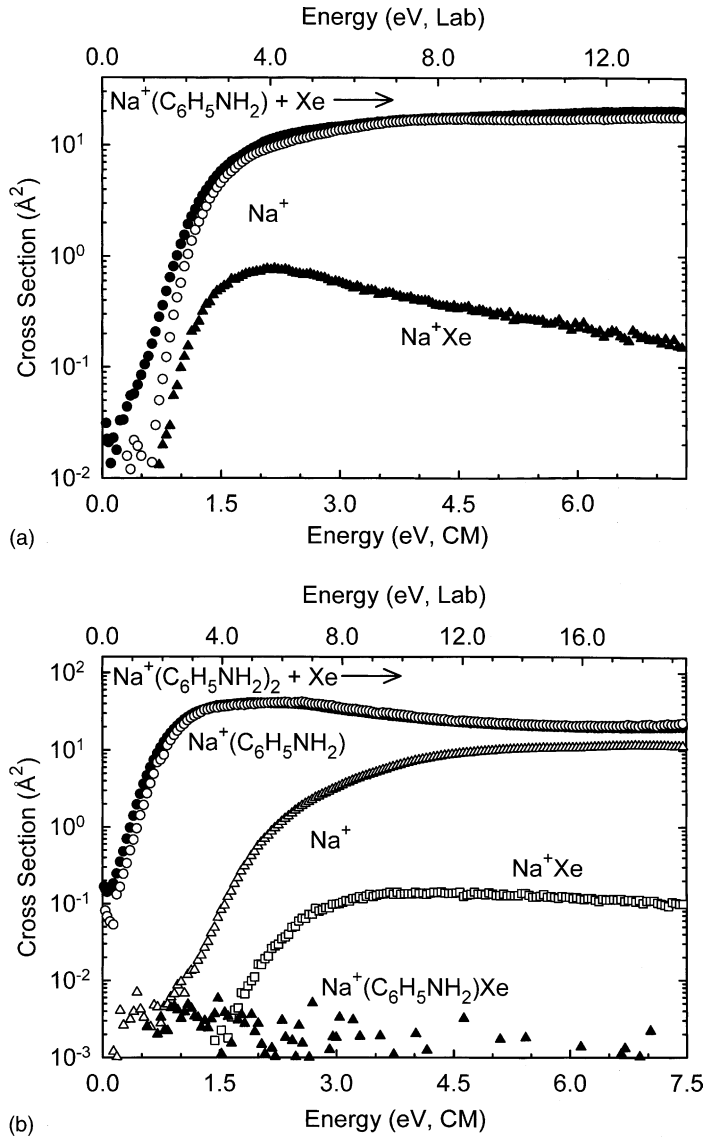

Fig. 2. Cross-sections for collision-induced dissociation of $Na^+(C_6H_5NH_2)_x$, where $x = 1$ and 2 (parts a and b, respectively), with Xe as a function of kinetic energy in the center-of-mass frame (lower *x*-axis) and the laboratory frame (upper *x*-axis). Data are shown for a Xe pressure of ~0.2 and ~0.1 mTorr for the $x = 1$ and 2 complexes, respectively. Primary and secondary product cross-sections are shown as ● and △, respectively. Primary and secondary ligand exchange product cross-sections are shown as ▲ and □, respectively. Data are also shown for the primary product cross-section, extrapolated to zero pressure of Xe as ○.

3.1.1. $M^+(C_6H_5NH_2) + Xe$

Results for the interaction of $Na^+(C_6H_5NH_2)$ with Xe are shown in Fig. 2a. The major product is Na^+, which exhibits an apparent threshold of 0.7 eV and a maximum cross-section of ~18 Å^2. The apparent thresholds for the analogous CID process in the other $M^+(C_6H_5NH_2)$ complexes decrease regularly as the size of the cation increases, such that $Li^+(C_6H_5NH_2)$ exhibits the largest apparent threshold of 2.1 eV, and $Cs^+(C_6H_5NH_2)$ the smallest apparent threshold of

<0.1 eV. In general, the cross-section maxima for other $M^+(C_6H_5NH_2)$ complexes increase with the size of the cation, such that cross-section maxima are the smallest for $Li^+(C_6H_5NH_2)$, ~2 Å^2, and the largest for $Cs^+(C_6H_5NH_2)$, ~24 Å^2. The $Rb^+(C_6H_5NH_2)$ complex deviates from this simple trend exhibiting a maximum cross-section of ~16 Å^2, similar to that observed for the Na^+ complex. The ligand exchange product Na^+Xe is observed with an apparent threshold of 0.8 eV and a maximum cross-section of 0.7 Å^2 at 2.3 eV, which drops off rapidly with energy due to competition with the primary CID process. The apparent thresholds for the analogous ligand exchange process of the other $M^+(C_6H_5NH_2)$ complexes decrease regularly as the size of the cation increases, such that Li^+Xe exhibits the largest apparent threshold of 1.5 eV, and $Cs^+(C_6H_5NH_2)$ the smallest apparent threshold of 0.1 eV. The cross-section maxima for other M^+Xe products are small and range from 0.3 to 0.8 Å^2 for other $M^+(C_6H_5NH_2)$ complexes.

3.1.2. $M^+(C_6H_5NH_2)_2 + Xe$

Results of the interaction of $Na^+(C_6H_5NH_2)_2$ with Xe are shown in Fig. 2b. The dominant product observed at all energies is $Na^+(C_6H_5NH_2)$, corresponding to the loss of an intact $C_6H_5NH_2$ molecule. The $Na^+(C_6H_5NH_2)$ product has an apparent threshold near or below 0 eV, such that the cross-section is nonzero at 0 eV. The apparent threshold for the analogous CID process in the other $M^+(C_6H_5NH_2)_2$ complexes exhibits similar behavior in that the cross-section magnitude is nonzero at 0 eV for all of the alkali metal ions except Li^+, which exhibits an apparent threshold of ~0.2 eV. In fact, the cross-section magnitude at 0 eV and all energies is found to increase with increasing size of the alkali metal ion and is more than twice as large as that measured for the $M^+(C_6H_5NH_2)$ complexes. However, the Rb^+ system again deviates from this trend, exhibiting a cross-section that is smaller than for any of the other metal ions. The maximum cross-section observed varies from 35 to 79 Å^2 across these systems. The cross-section for the primary product is observed to decline as the secondary CID product, Na^+ is formed, indicating that this product is formed sequentially from the primary CID product. The Na^+ product has an apparent threshold of 0.8 eV and reaches a maximum cross-section of ~11 Å^2 at the highest energies examined. The other $M^+(C_6H_5NH_2)_2$ complexes show similar behavior such that the primary product declines as the secondary CID product, M^+, appears. The cross-section maxima of the secondary CID products vary from 3 to 15 Å^2 across these systems.

In addition to the CID processes, ligand exchange reactions are also observed, producing both the primary ligand exchange product, $Na^+(C_6H_5NH_2)Xe$, as well as the secondary ligand exchange product, Na^+Xe (Fig. 2b). The primary ligand exchange product, $Na^+(C_6H_5NH_2)Xe$, has an apparent threshold near 0.4 eV, reaches a maximum cross-section of ~0.04 Å^2, and then falls off rapidly due to competition with the primary CID process, as well as sequential dissociation, to produce the secondary ligand exchange product, Na^+Xe. The secondary ligand exchange product, Na^+Xe, slowly grows in from an apparent threshold of ~1.4 eV, and reaches a maximum cross-section of ~0.2 Å^2 at approximately 3.8 eV. At higher energies, it falls off due to competition with the secondary CID process. The other $M^+(C_6H_5NH_2)_2$ complexes show similar ligand exchange behavior. However, the intensity of the primary ligand exchange product, $M^+(C_6H_5NH_2)Xe$, was much smaller for the complexes, where $M^+ = K^+$, Rb^+, Cs^+, making it impossible to distinguish this product from noise in these systems. The cross-section magnitudes of the ligand exchange products are quite small. The primary and secondary ligand exchange products are approximately 3 and 2 orders of magnitude smaller than the primary CID product, respectively.

3.2. Threshold analysis

The model of Eq. (1) was used to analyze the thresholds for reaction 2 in 10 $M^+(C_6H_5NH_2)_x$ systems. As previously discussed [57,60], the analysis of the primary CID thresholds provides the most reliable thermochemistry for such CID studies. This is because secondary and higher order products are

Table 3
Fitting parameters of Eq. (1), threshold dissociation energies at 0 K, and entropies of activation at 1000 K[a]

Reactant complex	σ_0[b]	n[b]	E_0[c] (eV)	E_0(PSL) (eV)	Kinetic shift (eV)	$\Delta S^{\dagger}$(PSL) (J K^{-1} mol^{-1})
$Li^+(C_6H_5NH_2)$	0.7 (0.2)	1.6 (0.1)	2.23 (0.29)	1.98 (0.23)	0.25	43 (2)
$Na^+(C_6H_5NH_2)$	20.4 (1.0)	1.1 (0.1)	1.27 (0.03)	1.24 (0.03)	0.03	41 (2)
$K^+(C_6H_5NH_2)$	22.8 (0.3)	1.2 (0.1)	0.86 (0.03)	0.86 (0.03)	0.00	37 (2)
$Rb^+(C_6H_5NH_2)$	21.5 (0.3)	1.4 (0.1)	0.79 (0.04)	0.79 (0.05)	0.00	60 (2)
$Cs^+(C_6H_5NH_2)$	39.0 (3.0)	1.3 (0.1)	0.73 (0.05)	0.73 (0.05)	0.00	49 (2)
$Li^+(C_6H_5NH_2)_2$	55.2 (1.3)	1.0 (0.1)	1.57 (0.05)	1.33 (0.04)	0.24	48 (5)
$Na^+(C_6H_5NH_2)_2$	82.7 (3.6)	1.0 (0.2)	1.11 (0.05)	1.02 (0.05)	0.09	40 (5)
$K^+(C_6H_5NH_2)_2$	79.0 (2.1)	1.1 (0.1)	0.84 (0.05)	0.79 (0.03)	0.05	14 (5)
$Rb^+(C_6H_5NH_2)_2$	56.4 (3.1)	1.1 (0.1)	0.78 (0.07)	0.74 (0.03)	0.04	10 (9)
$Cs^+(C_6H_5NH_2)_2$	119.6 (5.2)	1.1 (0.1)	0.72 (0.08)	0.68 (0.03)	0.04	10 (9)

[a] Uncertainties are listed in parentheses.
[b] Average values for loose PSL transition state.
[c] No RRKM analysis.

more sensitive to lifetime effects, and additional assumptions are needed to quantitatively include the multiple products formed. The results of these analyses are given in Table 3 for all 10 $M^+(C_6H_5NH_2)_x$ complexes. Representative fits using Eq. (1) for $Na^+(C_6H_5NH_2)_x$, $x = 1$ and 2, are shown in Fig. 3. Experimental cross-sections for the primary dissociation processes of the $M^+(C_6H_5NH_2)_x$ complexes are accurately reproduced using a loose PSL TS model [39]. This model has been shown to provide the most accurate determination of kinetic shifts for CID reactions for electrostatically bound metal–ligand complexes [35,39,64,65,80–83]. The data is accurately reproduced over energy ranges exceeding 1 eV and over cross-section magnitudes of a factor of at least 100 for all complexes except $Rb^+(C_6H_5NH_2)_2$ and $Cs^+(C_6H_5NH_2)_2$ because these cross-sections are already nonzero at 0 eV. Threshold values, E_0 and E_0(PSL), obtained from analyses of the data with and without explicit consideration of lifetime effects are also included in Table 3. The difference between these threshold values, the kinetic shift, is also given in Table 3. The kinetic shifts observed for these systems vary from 0.0 to 0.25 eV for the $M^+(C_6H_5NH_2)$ complexes with 39 vibrational modes, and from 0.04 to 0.24 eV for the $M^+(C_6H_5NH_2)_2$ complexes which have 81 vibrational modes. The kinetic shifts decrease with increasing size of the cation, from Li^+ to Cs^+, in both the mono- and bis-complexes. This is easily understood because the observed kinetic shift should directly correlate with the density of states of the complex at threshold, which depends upon the measured BDE, as shown in Table 3.

The entropy of activation, $\Delta S^{\dagger}$, is a measure of the looseness of the TS. It is also a reflection of the complexity of the system because it is largely determined by the molecular parameters used to model the energized molecule and the TS, but also depends upon the threshold energy. The $\Delta S^{\dagger}$(PSL) values at 1000 K are listed in Table 3 and vary between 10 and 60 J K^{-1} mol^{-1}. These entropies of activation compare favorably to an expanding range of noncovalently bound metal–ligand complexes previously measured in our laboratory and to those collected by Lifshitz for simple bond cleavage reactions of ions [84].

3.3. Theoretical results

Theoretical structures for neutral $C_6H_5NH_2$ and for the $M^+(C_6H_5NH_2)_x$ complexes, where $M^+ = Li^+$, Na^+, K^+, Rb^+, and Cs^+, and $x = 1$ and 2, were calculated as described earlier. Details of the geometry-optimized structures for each of these species are given in Table 4. The most stable structures for the $Na^+(C_6H_5NH_2)$ and $Na^+(C_6H_5NH_2)_2$ complexes are shown in Fig. 4. The metal atom binds

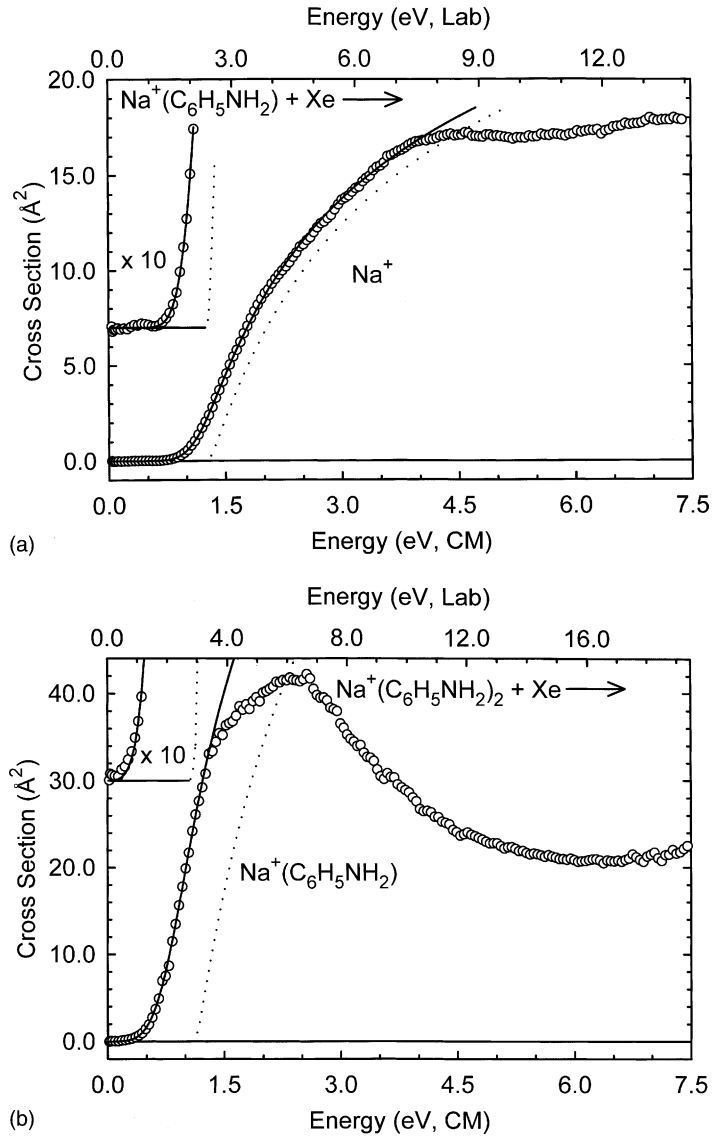

Fig. 3. Zero-pressure extrapolated cross-sections for the primary collision-induced dissociation product of the $Na^+(C_6H_5NH_2)_x$ complexes, $x = 1$ and 2 (parts a and b, respectively), with Xe in the threshold region as a function of kinetic energy in the center-of-mass frame (lower x-axis) and the laboratory frame (upper x-axis). Solid lines show the best fits to the data using the model of Eq. (1) convoluted over the neutral and ion kinetic and internal energy distributions. Dashed lines show the model cross-sections in the absence of experimental kinetic energy broadening for reactants with an internal energy of 0 K.

to the π cloud of the aromatic ring of the aniline molecule, a cation-π interaction. The distortion of the aniline molecule that occurs upon complexation to the alkali metal ion is minor. The change in geometry is largest for Li^+ and decreases with increasing size of the metal ion. The C–C bond lengths in the aromatic ring of aniline were found to increase by 0.003–0.012 Å upon complexation to the alkali metal ion as compared to the free ligand (Table 4). The alkali metal ion appears to have no influence on the

Table 4
Geometrical parameters of B3LYP/6-31G* optimized structures of the $M^+(C_6H_5NH_2)_x$ complexes

Complex	M^+–C (Å)	M^+–ring-centroid[a] (Å)	M^+–N (Å)	C–C (Å)	C–H (Å)	CHOOP angle[b] (°)	C–NH_2 (Å)	N–H (Å)
$C_6H_5NH_2$				1.398	1.090	0.300	1.400	1.013
$Li^+(C_6H_5NH_2)$	2.336	1.873		1.410	1.090	1.070	1.362	1.011
$Li^+(C_6H_5NH_2)$[c]			1.978	1.399	1.090	0.805	1.449	1.020
$Na^+(C_6H_5NH_2)$	2.740	2.355		1.407	1.090	0.718	1.376	1.012
$Na^+(C_6H_5NH_2)$[c]			2.360	1.399	1.090	0.741	1.441	1.019
$K^+(C_6H_5NH_2)$	3.164	2.834		1.404	1.090	0.378	1.387	1.013
$K^+(C_6H_5NH_2)$[c]			2.863	1.399	1.090	0.551	1.427	1.018
$Rb^+(C_6H_5NH_2)$[d]	3.440	3.129		1.403	1.090	0.303	1.394	1.014
$Rb^+(C_6H_5NH_2)$[c,d]			3.102	1.399	1.090	0.502	1.425	1.018
$Cs^+(C_6H_5NH_2)$[d]	3.748	3.393		1.401	1.090	0.206	1.404	1.015
$Cs^+(C_6H_5NH_2)$[c,d]			3.378	1.399	1.090	0.341	1.421	1.017
$Li^+(C_6H_5NH_2)_2$	2.481	2.044		1.406	1.090	0.455	1.375	1.012
$Na^+(C_6H_5NH_2)_2$	2.812	2.437		1.405	1.090	0.433	1.381	1.012
$K^+(C_6H_5NH_2)_2$	3.214	2.890		1.404	1.090	0.269	1.389	1.013
$Rb^+(C_6H_5NH_2)_2$[d]	3.472	3.185		1.403	1.090	0.241	1.396	1.014
$Cs^+(C_6H_5NH_2)_2$[d]	4.077	3.428		1.400	1.090	0.279	1.417	1.017

[a] The metal–ring-centroid distance is defined as the distance from the metal atom to the central point within the aromatic ring of aniline that is in the plane of the carbon atoms.
[b] Out-of-plane angle.
[c] Cation-π complexes in which the alkali metal ion interacts with the amino substituent.
[d] The Hay–Wadt ECP/valence basis set was used for the metal ion, as described in the text, and the 6-31G* basis set for C and H.

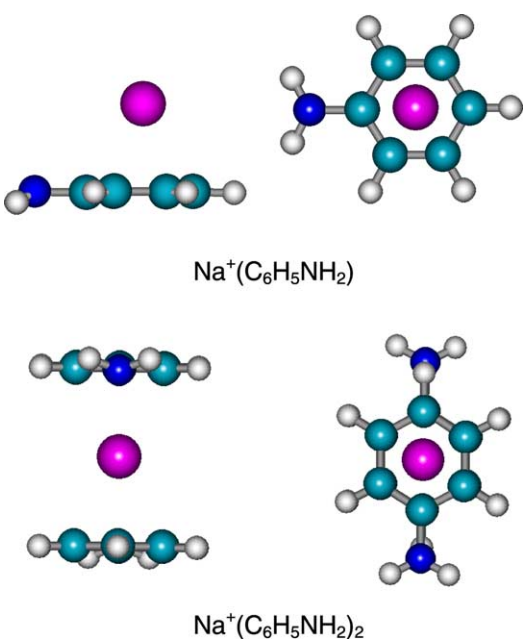

Fig. 4. Ground state B3LYP/6-31G* optimized geometries of $Na^+(C_6H_5NH_2)_x$ cation-π complexes, where $x = 1$ and 2. Two views of each optimized structure are shown.

C–H bond lengths (1.090 Å). The C–N bond length was found to decrease upon complexation to all of the alkali metal ions except Cs^+. This effect is larger for the mono-ligated complexes (0.006–0.038 Å) than for the bis-ligated complexes (0.004–0.025 Å), and decreases with increasing size of the alkali metal ion. Thus, the cation-π interaction leads to more double bond character in the C–N bond, resulting in an enhancement of the π electron density of the aromatic ring. The N–H bond lengths are slightly influenced by complexation and were found to change by 0.002–0.004 Å. As summarized in Table 4, the M^+–C and M^+–ring-centroid distances[2] are found to increase as the size of the metal ion increases from Li^+ to Cs^+ for both the mono- and bis-complexes. The M^+–C and M^+–ring-centroid distances are also found to increase on going from the mono-complex to the corresponding bis-complex, for all metal ions, as expected for electrostatically bound complexes. In

[2] The metal–ring-centroid distance is defined as the distance from the metal atom to the central point within the aromatic ring that lies in the plane of the carbon atoms.

contrast to that found for the analogous benzene systems [9], out-of-plane bending of the ring hydrogen atoms is found to decrease with increasing size of the alkali metal ion, and is smaller for the bis-complexes than for the mono-complexes. This makes sense because the alkali metal ion is further away from the ring, and therefore, these hydrogen atoms in the complexes to the larger metal ions. The metal ion is also further from these atoms in the bis-complexes than in the mono-complexes, and should therefore, exert a smaller influence on the ligand.

As can be seen in Fig. 4, the ground state structure of $Na^+(C_6H_5NH_2)$ has the Na^+ ion interacting with the π cloud of the aromatic ring such that it sits very close to the center of the ring. However, it is possible that the alkali metal ion might interact with the amino substituent. Because the amino substituent is very nearly planar, the lone pair of electrons on the N atom is oriented in the direction perpendicular to the plane of the molecule, the direction of the π space. This allows the amino substituent to delocalize some of its electron density into the π system and increases the resonance stabilization of the aniline molecule as shown by the Lewis structures below.Thus, com-

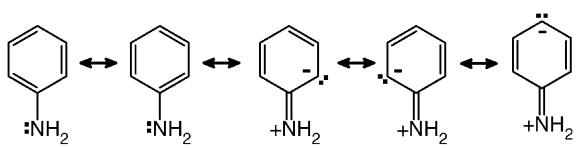

plexes in which the alkali metal ion interacts with the amino substituent are also cation-π complexes. Stable cation-π conformers in which the alkali metal ion interacts with the substituent were also found for the $M^+(C_6H_5NH_2)$ complexes for all of the alkali metal ions. The optimized structure of the corresponding $Na^+(C_6H_5NH_2)$ complex is shown in Fig. 5. The alkali metal ion lies above the C–N bond and interacts with its π electrons. It is interesting to note that in these complexes, the alkali metal ion is oriented to allow efficient interaction with the dipole moment of the aniline ligand. At the MP2(full)/6-311+G(2d,2p) level of theory, these conformers are found to be 8.6, 1.6, 2.8, 1.0, and 1.4 kJ mol^{-1} less stable than the

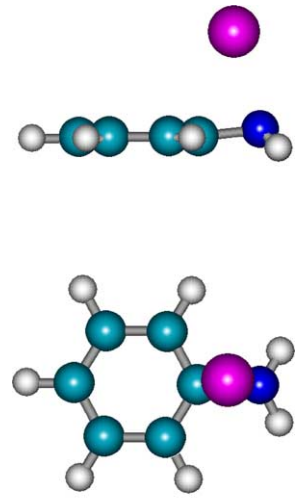

Fig. 5. B3LYP/6-31G* optimized geometry of the cation-π conformer of $Na^+(C_6H_5NH_2)$ in which Na^+ binds to the amino substituent. Two views of the optimized structure are shown.

ground state conformers for Li^+, Na^+, K^+, Rb^+, and Cs^+, respectively. The small difference in stability of these and the ground state conformers suggests that these conformers should have sufficient internal energy at room temperature to freely interconvert for all of the alkali metal ions.

It might also be possible for the alkali metal ion to interact with the amino substituent in the plane of the molecule. However, such σ-binding complexes would be expected to be much less stable than the cation-π complexes because such complexation requires that the amino group rotate out of the plane of the molecule, and rehybridize from sp^2 to sp^3. Such rehybridization results in a significant loss of π-resonance delocalization energy. In earlier work, we examined the binding of alkali metal ions to adenine [42]. The ground state geometry of these complexes involved binding to the N7, imidazolic nitrogen atom, with an additional chelation interaction to the amino group attached to the C6 position. In this work, we found that the energetic cost of rotating the amino group of adenine out of the plane to allow this chelation interaction to occur was independent of the metal ion and

cost ~55 kJ mol^{-1}. Because the interaction of the alkali metal ion with aniline in the cation-π complexes involves more than the lone pair of electrons on the N atom, it is anticipated that planar σ-binding complexes to aniline are likely to be at least 55 kJ mol^{-1} less stable than the cation-π complexes. Attempts to calculate stable σ-binding conformers in which the alkali metal ion interacts with the amino substituent in the plane of the aromatic ring always converged to the energetically more favorable cation-π complexes in which the alkali metal ion interacts with the amino group. Therefore, we can safely assume that such conformers are unimportant in the binding of alkali metal ions to aniline.

As can be seen in Fig. 4, the lowest energy structure for the $Na^+(C_6H_5NH_2)_2$ complex has the amine substituents oriented anti to one another to minimize repulsive ligand–ligand interactions associated with the amine substituents. The anti configuration was found to be the lowest energy structure for all of the bis-complexes. To estimate the barrier to free rotation of the aromatic ring in the bis-complexes, optimizations were also performed for $Li^+(C_6H_5NH_2)_2$ with the amine groups oriented *syn*, "*ortho*", and "*meta*" to one another. These complexes were found to be 5.5, 1.0, and 0.3 kJ mol^{-1} less stable than when oriented anti to one another (excluding BSSE corrections). Therefore, at room temperature these complexes should have sufficient energy to freely interconvert (see Table 1).

Theoretical estimates for the $M^+(C_6H_5NH_2)_x$ BDEs were determined using the B3LYP/6-31G* geometries and single point energy calculations at the MP2(full)/6-311+G(2d,2p) level of theory. In earlier work in which we measured and calculated the

Table 5
Bond dissociation enthalpies of $M^+(C_6H_5NH_2)_x$, $x = 1$ and 2, at 0 K (kJ mol^{-1})

Complex	Experiment (TCID)		Theory (X = F)			
	X = NH_2[a]	X = H[b]	D_e[c]	D_0[c,d]	$D_{0,\,BSSE}$[c,e]	D_e
$Li^+(C_6H_5X)$	191.5 (22.4)	161.1 (13.5)	186.8	179.7	169.4	
			176.3[f]	168.3[f]	160.8[f]	
$Na^+(C_6H_5X)$	119.9 (2.7)	92.6 (5.8)	125.6	121.5	111.0	146.9[g]
		88.3 (4.3)[h]				133.0[i]
			123.2[f]	118.1[f]	109.4[f]	
$K^+(C_6H_5X)$	82.5 (3.2)	73.3 (3.8)	99.9	96.4	90.4	
			97.3[f]	93.2[f]	87.6[f]	
$Rb^+(C_6H_5X)$[j]	76.3 (4.5)	68.5 (3.8)	84.7	81.8	74.6	
			84.5[f]	80.8[f]	73.6[f]	
$Cs^+(C_6H_5X)$[j]	69.3 (4.2)	64.6 (4.8)	77.3	74.5	67.4	
			76.1[f]	72.8[f]	66.0[f]	
$Li^+(C_6H_5X)_2$	127.9 (3.7)	104.2 (6.8)	147.1	144.0	122.5	
$Na^+(C_6H_5X)_2$	98.8 (2.2)	80.0 (5.8)	111.0	107.9	91.8	
$K^+(C_6H_5X)_2$	75.9 (2.9)	67.5 (6.8)	89.1	86.5	75.9	
$Rb^+(C_6H_5X)_2$[j]	71.8 (2.7)	62.7 (7.7)	84.6	81.8	70.0	
$Cs^+(C_6H_5X)_2$[j]	66.1 (3.3)	58.8 (7.7)	69.2	66.8	57.8	

[a] Present results, threshold collision-induced dissociation. Uncertainties are listed in parentheses.
[b] Taken from Amicangelo and Armentrout, except as noted [9].
[c] Calculated at the MP2(full)/6-311+G(2d,2p) level of theory using B3LYP/-31G* optimized geometries.
[d] Including zero point energy corrections with B3LYP/6-31G* frequencies scaled by 0.9804.
[e] Also, includes basis set superposition error corrections.
[f] Cation-π conformer in which the alkali metal ion interacts with the amino substituent.
[g] Mecozzi et al. calculated at the MP2/6-31G**//HF/6-31G** level of theory [14].
[h] Armentrout and Rodgers [8].
[i] Mecozzi et al. calculated at the HF/6-31G**//HF/6-31G** levels of theory [14].
[j] The Hay–Wadt ECP/valence basis set was used for the metal ion, as described in the text, and the 6-31G* basis set and 6-311+G(2d,2p) basis set were used for C, N, and H in geometry optimizations and single point energy calculations, respectively.

strength of cation-π interactions of $M^+(C_6H_5CH_3)_x$ complexes, we found much better correlation between theoretical and experimental results for energetics based on MP2(full)/6-311+G(2d,2p) theory than for B3LYP/6-311+G(2d,2p) theory. In this earlier work, the MP2 results exhibit a mean absolute deviation (MAD) of $10.2 \pm 7.3\,kJ\,mol^{-1}$; whereas the B3LYP results exhibit an MAD of $19.3 \pm 6.9\,kJ\,mol^{-1}$. We have, therefore, employed the former in the present work [11]. These results are listed in Table 5 along with the experimental determinations performed here for aniline, and other theoretical results found in the literature [14]. Results shown in Table 5 also include ZPE and BSSE corrections.

4. Discussion

4.1. Trends in experimental $M^+(C_6H_5NH_2)_x$ BDEs

The experimental BDEs of the $M^+(C_6H_5NH_2)_x$ complexes at 0 K are summarized in Table 5. The variation in the measured BDEs with the size of the alkali metal ion is shown in Fig. 6 for both the mono- and bis-ligated complexes. The M^+–$(C_6H_5NH_2)$ and $(C_6H_5NH_2)M^+$–$(C_6H_5NH_2)$ BDEs are found to decrease monotonically as the size of the alkali metal increases from Li^+ to Cs^+. Similar trends were observed for the analogous benzene [9], toluene [11], and fluorobenzene [12] systems. This is the expected trend for binding based primarily on electrostatic interactions (ion–dipole, ion–quadrupole, and ion-induced dipole) [19], because the increasing size of the alkali metal ion [85] leads to larger metal–ligand bond distances (see Table 4). In addition, the difference in BDEs for adjacent metals becomes smaller as the size of the metal ion increases from Li^+ to Cs^+ for both the $M^+(C_6H_5NH_2)$ and $M^+(C_6H_5NH_2)_2$ complexes. This trend results from a combination of two factors. First, the relative change in ionic radii for the alkali metal ions becomes smaller as the size of the cation increases (0.68, 0.97, 1.33, 1.47, and 1.67 Å for Li^+, Na^+, K^+, Rb^+, and Cs^+, respectively) [85]. Second, the nonlinear distance dependencies of the electrostatic interactions fall off rapidly as R^{-2} for ion–dipole, as R^{-3} for the ion–quadrupole, and as R^{-4} for ion-induced dipole interactions.

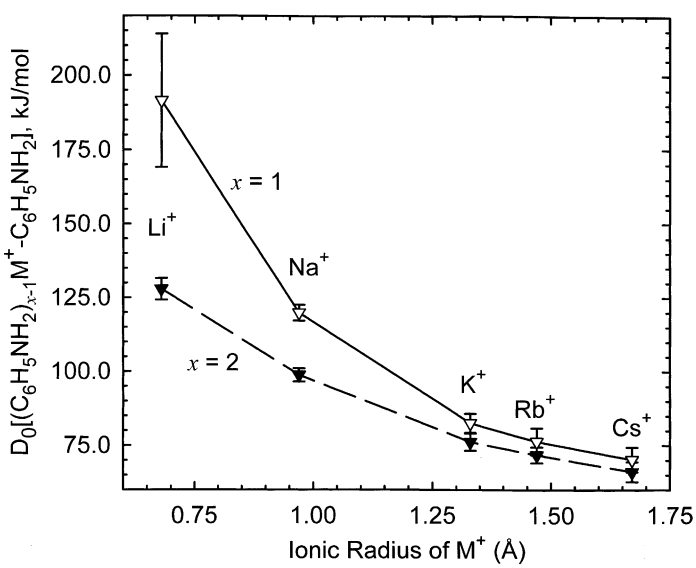

Fig. 6. Bond dissociation energies at 0 K (in $kJ\,mol^{-1}$) of the $M^+(C_6H_5NH_2)_x$ complexes plotted vs. the ionic radius of M^+. Data are shown for $x = 1$ and 2 as ▽ and ▼, respectively. All values are taken from Table 5.

The BDEs of the bis-complexes are smaller than the BDEs for the corresponding mono-complexes in all cases. The decrease in the measured BDE on going from the mono- to the corresponding bis-complex is largest for Li^+, and decreases with increasing size of the alkali metal ion. The sequential BDEs are observed to decrease by 64.6, 21.1, 6.6, 4.5, and 3.2 kJ mol^{-1} for the Li^+, Na^+, K^+, Rb^+, and Cs^+ systems, respectively. Similar trends were observed for the analogous benzene [9], toluene [11], and fluorobenzene [12] systems. This trend is believed to be the result of Coulombic and dipole–dipole repulsions between the ligands [80]. The distance between the aromatic rings is found to increase with increasing size of the alkali metal ion, from ∼ 4.08 Å in $Li^+(C_6H_5NH_2)_2$ to 6.86 Å in $Cs^+(C_6H_5NH_2)_2$ (Table 4, 2 × M^+–ring-centroid distance). The magnitude of the repulsive ligand–ligand interactions should decrease with increasing separation of the ligands. This should result in smaller differences in the BDEs for the mono- and bis-complexes with increasing size of the alkali metal ion, as observed. The very small differences observed for the K^+, Rb^+, and Cs^+ systems suggest that the ligand–ligand repulsions are very similar and minor for these complexes.

4.2. Comparison of theory and experiment

The experimentally determined and theoretically calculated $M^+(C_6H_5NH_2)_x$ BDEs are listed in Table 5. The agreement between the experimental BDEs and theoretical values determined at the MP2(full)/6-311+G(2d,2p)//B3LYP/6-31G* level is illustrated in Fig. 7. BDEs determined from the theoretical calculations are in good agreement with the measured BDEs. The MAD between the experimental and theoretical values for all 10 complexes is 6.5 ± 6.4 kJ mol^{-1}. This is slightly greater than the average experimental error of 5.2 ± 6.1 kJ mol^{-1}. The MAD is larger for the mono-ligated complexes, 8.5 ± 8.3 kJ mol^{-1}, than for the bis-ligated complexes, 4.5 ± 3.5 kJ mol^{-1}. However, the calculated values for the Li^+, Na^+, and K^+ complexes are expected to be more accurate than those for the Rb^+ and Cs^+ complexes because the latter make use of ECPs to describe the alkali metal ion. Therefore, it is more informative to examine these systems individually. The agreement between the experimental and the six theoretical $M^+(C_6H_5NH_2)_x$ BDEs calculated, including all electrons ($M^+ = Li^+$, Na^+, K^+, $x = 1$ and 2), is reasonably good, with an MAD of 8.6 ± 7.3 kJ mol^{-1}. These differences are somewhat larger than the average experimental error in these values of 6.2 ± 8.0 kJ mol^{-1}. Inspection of the data makes it clear that the Li^+ complex is the principal contributor to the MAD for these complexes. This poorer agreement may arise for two reasons. The first is the experimental difficulty in measuring cross-sections for Li^+ as a result of the difficulty associated with efficient detection of this light mass [47]. An alternative explanation is that theory may systematically underestimate the bond energies for Li^+ complexes, as a result of the higher degree of covalency in the metal–ligand bond. This is shown by the calculated partial charge on M^+, which is 0.78*e* for $Li^+(C_6H_5NH_2)$ and varies between 0.90 and 0.99*e* for all of the other $M^+(C_6H_5NH_2)_x$ complexes at the

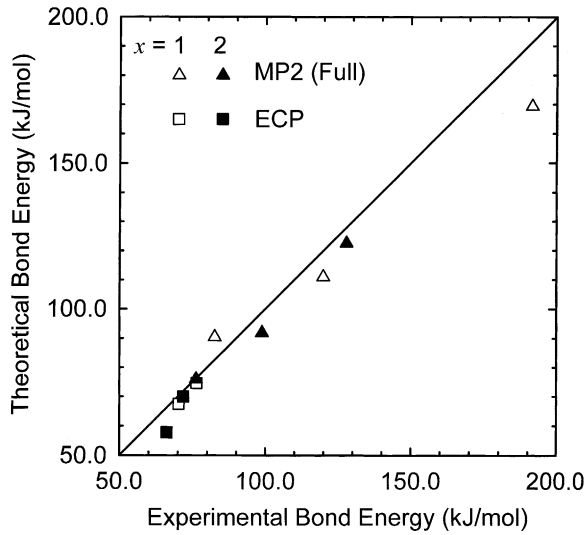

Fig. 7. Theoretical vs. experimental bond dissociation energies at 0 K (in kJ mol^{-1}) of the $M^+(C_6H_5NH_2)_x$ complexes. The diagonal line indicates the values for which the calculated and measured bond dissociation energies are equal. All values are taken from Table 5.

MP2(full)/6-311+G(2d,2p) level. Therefore, higher levels of theory may be required to accurately describe the binding in this complex, a conclusion also drawn for Li^+ complexes with a variety of other ligands [42,44,46]. If the $Li^+(C_6H_5NH_2)$ value is not included, the MAD drops to $5.8 \pm 3.5\,kJ\,mol^{-1}$, a much more reasonable value. The average experimental error also decreases to $2.9 \pm 0.6\,kJ\,mol^{-1}$ because the experimental error in the measured $Li^+(C_6H_5NH_2)$ value is much larger than for the other complexes.

Previous calculations for the $Na^+(C_6H_5NH_2)$ complex were performed at the MP2/6-31G**//HF/6-31G** and HF/6-31G**//HF/6-31G** levels of theory by Mecozzi et al. [14]. These values differ somewhat from the values obtained here. Both of their values are greater than that calculated here by 21.3 and $7.4\,kJ\,mol^{-1}$, respectively.[3] These differences are quite reasonable, based upon the expected accuracy of these levels of theory.

The agreement between the experimental BDEs and the theoretical values calculated using the Hay–Wadt ECP/valence basis set for the Rb^+ and Cs^+ complexes is surprisingly good and better than that found for the toluene [11] and fluorobenzene [12] systems. A MAD of $3.4 \pm 3.3\,kJ\,mol^{-1}$ is found. This is slightly smaller than the average experimental error in these values $3.7 \pm 0.8\,kJ\,mol^{-1}$. Consistent with the analogous benzene [9], toluene [11], and fluorobenzene [12] systems, the Hay–Wadt ECP/valence basis set results in calculated BDEs that are systematically lower than the experimental values.

4.3. Conversion from 0 to 298 K

To allow comparison to commonly used experimental conditions, we convert the 0 K bond energies determined here to 298 K bond enthalpies and free energies. The enthalpy and entropy conversions are calculated using standard formulas (assuming harmonic oscillator and rigid rotor models) and the vibrational and rotational constants determined for the B3LYP/6-31G* optimized geometries, which are given in Tables 1 and 2. Table 6 lists 0 and 298 K enthalpies, free energies, and enthalpic and entropic corrections for all systems experimentally determined (from Table 5). The uncertainties in the enthalpic and entropic corrections are determined by 10% variation in the molecular constants for complexes to Li^+, Na^+, and K^+, and by 20% variation in the molecular constants for complexes to Rb^+ and Cs^+. Because the metal–ligand frequencies are very low and may not be adequately described by theory, the listed uncertainties also include contributions from scaling these frequencies up and down by a factor of 2. The latter provides a conservative estimate of the computational errors in these low-frequency modes and is the dominant source of the uncertainties listed.

4.4. The influence of the amino substituent

The effect of the amino substituent on the cation-π interaction can be examined by comparing the results obtained here for aniline, $C_6H_5NH_2$, to those obtained in earlier studies for benzene [9], toluene [11], and fluorobenzene [12]. As can be seen in Fig. 8, the methyl and amino substituents result in an increase in the strength of the cation-π interaction, whereas the fluoro substituent produces a decrease in the strength of the cation-π interaction as compared to benzene. These observations can be understood by examining the influence of each of these substituents on the dipole moment, quadrupole moment, and polarizability of the aromatic ligand.

Benzene is a highly symmetric molecule and has no dipole moment. Substitution of one of the hydrogen atoms of the benzene ring by a substituent breaks up the symmetry in the molecule and results in a dipole moment regardless of the nature of the substituent. However, the magnitude and direction of the dipole moment is quite sensitive to the nature of the substituent. In toluene, the methyl substituent has only a minor effect and results in measured and calculated dipole moments of 0.36 ± 0.05 [50] and 0.41 D, respectively. In contrast, the amino and fluoro

[3] These differences represent differences in D_e because Mecozzi et al. did not include ZPE and BSSE corrections in the calculated binding energies they reported.

Table 6
Enthalpies and free energies of binding of $M^+(C_6H_5NH_2)_x$, $x = 1$ and 2, at 0 and 298 K (kJ mol^{-1})[a]

Reactant complex	ΔH_0[b]	$\Delta H_{298}-\Delta H_0$[c]	ΔH_{298}	$T\Delta S_{298}$[c]	ΔG_{298}
$Li^+(C_6H_5NH_2)$	191.5 (22.4)	3.0 (2.8)	194.5 (22.5)	30.8 (6.4)	16.3.7 (23.4)
$Na^+(C_6H_5NH_2)$	119.9 (2.7)	1.3 (2.0)	121.2 (3.4)	28.9 (7.0)	92.3 (7.7)
$K^+(C_6H_5NH_2)$	82.5 (3.2)	0.8 (1.8)	83.4 (3.7)	27.2 (6.9)	56.2 (7.9)
$Rb^+(C_6H_5NH_2)$	76.3 (4.5)	0.6 (1.6)	76.9 (4.8)	27.9 (7.8)	49.0 (9.2)
$Cs^+(C_6H_5NH_2)$	70.3 (4.2)	0.5 (1.8)	70.8 (4.5)	28.2 (7.7)	42.6 (9.0)
$Li^+(C_6H_5NH_2)_2$	127.9 (3.7)	−3.0 (1.9)	124.8 (4.2)	37.1 (12.3)	87.7 (12.9)
$Na^+(C_6H_5NH_2)_2$	98.8 (2.2)	−2.9 (1.7)	95.9 (2.8)	35.1 (12.2)	60.8 (12.5)
$K^+(C_6H_5NH_2)_2$	76.1 (2.9)	−3.2 (1.0)	72.9 (3.1)	28.1 (12.4)	44.8 (12.8)
$Rb^+(C_6H_5NH_2)_2$	71.8 (2.7)	−3.3 (1.2)	68.4 (2.9)	26.8 (13.7)	41.6 (14.0)
$Cs^+(C_6H_5NH_2)_2$	66.1 (3.3)	−3.4 (1.1)	62.7 (3.5)	26.5 (13.8)	36.2 (14.2)

[a] Uncertainties are listed in parentheses.
[b] Present experimental results (Table 5).
[c] Density functional values from calculations at the B3LYP/6-31G* level of theory with frequencies scaled by 0.9804. The Hay–Wadt ECP/valence basis set was used for Rb^+ and Cs^+.

substituents perturb the molecule to a much greater extent, resulting in relatively large dipole moments for aniline and fluorobenzene. The measured values of the dipole moments of aniline and fluorobenzene are 1.53 ± 0.02 and 1.60 ± 0.08 D, respectively [50].

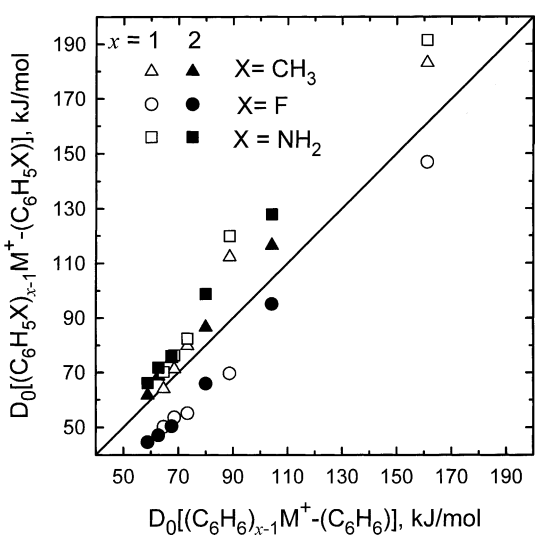

Fig. 8. Experimental bond dissociation energies at 0 K (in kJ mol^{-1}) of $(C_6H_5X)_{x-1}M^+$–(C_6H_5X) vs. $(C_6H_6)_{x-1}M^+$–(C_6H_6), where X = NH_2 (□, ■), CH_3 (△, ▲), and F (○, ●), and $M^+ = Li^+$, Na^+, K^+, Rb^+, and Cs^+. Data are shown for $x = 1$ and 2, respectively. Values for C_6H_6 are taken from Amicangelo and Armentrout [9]. Values for $C_6H_5CH_3$ and C_6H_5F are taken from and Amunugama and Rodgers [11,12], respectively.

The measured value for aniline is in good agreement with the value calculated here, 1.47 D. However, the value for fluorobenzene is significantly lower than the value determined from theoretical calculation, 1.91 D [11]. However, both the magnitude and the direction of the dipole moment is important. In toluene and fluorobenzene, the dipole moment lies in the plane of the aromatic ring and thus an effective interaction of the alkali metal ion with the dipole moment is not possible in cation-π complexes to these ligands. In contrast, the dipole moment of aniline is oriented ∼45° out of the plane of the molecule and towards the amino substituent. Therefore, the binding interaction in the cation-π complexes to aniline should be enhanced by the ion–dipole interaction in these complexes, particularly for the cation-π complex in which the alkali metal ion interacts with the amino substituent.

The polarizability of benzene is estimated using the additivity method of Miller [51] to be 9.99 Å^3 and increases to 11.53 Å^3 for aniline and 12.26 Å^3 for toluene; whereas it decreases slightly for fluorobenzene to 9.86 Å^3, respectively. Therefore the ion-induced dipole interaction should result in stronger binding to the aniline and toluene complexes and slightly weaker binding to fluorobenzene compared to that observed for benzene, consistent with our observations. Dougherty and coworkers have argued that to first order, the major aspect of the cation-π interaction

results from the interaction of the cation with the large permanent quadrupole moment of the aromatic ligand [14,15,19,20]. However, established techniques for measuring the quadrupole moment require that the molecule have no dipole moment [86]. Therefore, of the aromatic ligands of interest here, benzene, toluene, fluorobenzene, and aniline, the quadrupole moment has only been determined for benzene (-8.69 D Å) [86]. The quadrupole moment is a measure of the distribution of charge within a molecule, relative to a particular axis. In the case of these aromatic ligands, this axis is the axis that passes through the center of the aromatic ring and perpendicular to the plane of the carbon atoms. The large negative value of the quadrupole moment measured for benzene results from the delocalized π electron density above and below the plane of the aromatic ring. The influence of the substituent on the permanent quadrupole moment of the aromatic ring can be estimated by considering the inductive effects of the substituent. Both methyl and amino substituents are generally referred to as electron donors because they result in an increase in the π electron density of the aromatic ring. However, the amino substituent leads to a much greater enhancement in the π electron density than does the methyl substituent because the lone pair of electrons on the N atom is delocalized over the aromatic ring as shown in the Lewis structures described earlier. Such delocalization is not possible for the methyl substituent. In contrast, the fluoro substituent is electron withdrawing and decreases the electron density of the aromatic π system, localizing more electron density in the plane of the aromatic ring. Thus, the quadrupole moments of these molecules should follow the order fluorobenzene < benzene < toluene < aniline. Therefore, to first order, the strength of the cation-π interaction should also follow this order.

As discussed earlier, a cation-π interaction between an alkali metal ion and an aromatic ligand is expected to be largely electrostatic, arising from ion–dipole, ion–quadrupole, and ion-induced dipole, but dominated by the ion–quadrupole interaction. All of these effects act in concert to increase the strength of the cation-π interaction in the toluene and aniline complexes. The effect is larger for aniline than toluene because aniline has a larger dipole moment that is oriented out of the plane of the ring and enhances the π electron density of the aromatic ring and thus the quadrupole moment to a much greater extent. In contrast, the smaller quadrupole moment and polarizability of fluorobenzene should weaken the binding to fluorobenzene. In this case, the large dipole moment of fluorobenzene is incapable of effectively interacting with the alkali metal ion because it lies in the plane of the aromatic ring. The measured BDEs of the $M^+(C_6H_5X)_x$ complexes correlate directly with the influence of the substituent on the electron density of the aromatic π system, and therefore, the quadrupole moment of the aromatic ligand as previously suggested. The BDEs to toluene show a slight increase, those to fluorobenzene show a modest decrease, and those to aniline show a modest increase compared to the analogous benzene complexes. The increase in the cation-π BDES to aniline, relative to those of benzene, varies between 4.7 and 30.4 kJ mol^{-1} for the mono-complexes and between 7.3 and 23.7 for the bis-complexes. The enhancement in the binding energy is greatest for the Li^+ complexes and decreases with increasing size of the cation. Likewise, the enhancement in binding is greater for the mono-ligated complexes than for the bis-ligated complexes for Li^+, Na^+, and K^+, but is slightly smaller for Rb^+ and Cs^+.

4.5. Comparison to M^+(aniline) complexes

As mentioned in the Section 1, only two studies of cation-π interactions to aniline have been reported. In fact, previous studies of the alkali metal ions interacting with aniline have been limited to theoretical calculations for Na^+ as discussed earlier. The other study of cation-π interactions to aniline involved experimental measurements of the binding to Cr^+, Fe^+, and Co^+ [7]. The binding in these complexes is expected to be somewhat different than to the alkali metal ions because these ions possess valence electrons that can participate in the binding interaction, resulting in much stronger BDEs. Compared to the BDEs to K^+, the alkali metal ion of the same period, these transition

metal ions bind to aniline much more strongly. The interaction with the valence electrons of these ions enhances the cation-π interaction by 104.9, 143.4, and 188.6 kJ mol^{-1} for Cr^+, Fe^+, and Co^+, respectively. Similar to that found here, aniline was also found to bind to all three transitional metal ions, Cr^+, Fe^+, and Co^+, more strongly than to benzene by 17.6, 18.4, and 15.5 kJ mol^{-1}, respectively. In fact, of the wide variety of mono-substituted benzenes we examined in this study, aniline was found to bind most strongly. This is consistent with the observations made for the alkali metal ions interacting with the aromatic ligands we have examined thus far.

5. Conclusions

The kinetic energy dependence of the CID of $M^+(C_6H_5NH_2)_x$ complexes ($M^+ = Li^+$, Na^+, K^+, Rb^+, and Cs^+, $x = 1$ and 2) with Xe is examined in a guided ion beam tandem mass spectrometer. The dominant dissociation pathway, observed for all mono- and bis-complexes, is the loss of an intact aniline molecule. Thresholds for these dissociation reactions are determined after careful consideration of the effects of reactant internal energy, multiple collisions with Xe, and the lifetime of the ionic reactants (using a loose PSL TS model). Molecular parameters needed for the analysis of experimental data, as well as structures and theoretical estimates of the BDEs, for the $M^+(C_6H_5NH_2)_x$ complexes are obtained from theoretical calculations performed at the MP2(full)/6-311+G(2d,2p)//B3LYP/6-31G* level. The agreement between theory and experiment is quite good when both full electron correlation (for Li^+, Na^+, and K^+) and ECPs (for Rb^+ and Cs^+) are used. However, larger deviations are observed for the mono-ligated Li^+ complex. The absolute M^+–$(C_6H_5NH_2)$ and $(C_6H_5NH_2)M^+$–$(C_6H_5NH_2)$ BDEs, as well as the change in sequential $M^+(C_6H_5NH_2)_x$ ($x = 1$ and 2) BDEs, are observed to decrease monotonically as the size of the alkali metal ion increases from Li^+ to Cs^+. These trends are explained in terms of the electrostatic nature of the bonding, primarily an ion–quadrupole interaction, in the $M^+(C_6H_5NH_2)_x$ complexes and the changes in magnitude of the repulsive ligand–ligand interactions in the bis-complexes. Comparisons made to experimental BDEs of the analogous benzene, toluene, and fluorobenzene complexes reveal that the amino substituent leads to the largest increase in the strength of the cation-π interaction, in both the mono- and bis-complexes, to all of the alkali metal ions in accord with its influence on the quadrupole moment of the aromatic ring.

Acknowledgements

This work was supported by the National Science Foundation Grant No. 0138504.

References

[1] V. Ryzhov, R.C. Dunbar, J. Am. Chem. Soc. 121 (1999) 2259.
[2] A. Gapeev, C.-N. Yang, S.J. Klippenstein, R.C. Dunbar, J. Phys. Chem. A 104 (2000) 3246.
[3] V. Ryzhov, R.C. Dunbar, B. Cerda, C. Wesdemiotis, J. Am. Soc. Mass Spectrom. 11 (2000) 1037.
[4] A. Gapeev, R.C. Dunbar, J. Am. Chem. Soc. 123 (2000) 8360.
[5] E.S. Meadows, S.L. De Wall, L.J. Barbour, G.W. Gokel, J. Am. Chem. Soc. 123 (2000) 3092.
[6] G.W. Gokel, S.L. De Wall, E.S. Meadows, Eur. J. Org. Chem. (2000) 2967.
[7] K. Schroeter, R. Wesendrup, H. Schwarz, Eur. J. Org. Chem. (1998) 565.
[8] P.B. Armentrout, M.T. Rodgers, J. Phys. Chem. A 104 (2000) 2238.
[9] J.C. Amicangelo, P.B. Armentrout, J. Phys. Chem. A 104 (2000) 11420.
[10] H. Huang, M.T. Rodgers, J. Phys. Chem. A 106 (2002) 4277.
[11] R. Amunugama, M.T. Rodgers, J. Phys. Chem. A 106 (2002) 5529.
[12] R. Amunugama, M.T. Rodgers, J. Phys. Chem. A 106 (2002) 9092.
[13] S.D. Zaric, D.M. Popovic, E.-W. Knapp, Chem. Eur. J. 6 (2000) 3935.
[14] S. Mecozzi, P.A. West Jr., D.A. Dougherty, J. Am. Chem. Soc. 118 (1996) 2307.
[15] J.P. Gallivan, D.A. Dougherty, Proc. Natl. Acad. Sci. U.S.A. 96 (1999) 9459.
[16] R.C. Dunbar, J. Phys. Chem. A 104 (2000) 8067.
[17] D. Feller, D.A. Dixon, J.B. Nicholas, J. Phys. Chem. A 104 (2000) 11414.

[18] S. Tsuzuki, M. Yoshida, T. Uchimaru, M. Mikami, J. Phys. Chem. A 105 (2001) 769.
[19] J.C. Ma, D.A. Dougherty, Chem. Rev. 97 (1997) 1303.
[20] D.A. Dougherty, Science 271 (1996) 163.
[21] J. Sunner, K. Nishizawa, P. Kebarle, J. Phys. Chem. 85 (1981) 1814.
[22] S.J. Lippard, J.M. Berg (Eds.), Principles of Bioinorganic Chemistry, University Science Books, Mill Valley, CA, 1994.
[23] A.H. Bond, M.L. Dietz, R.D. Rodgers (Eds.), Metal-Ion Separation and Preconcentration, ACS Symposium Series 716, American Chemical Society, Washington, DC, 1999.
[24] A.M. DeVos, M. Ultsch, A.A. Kossiakoff, Science 255 (1992) 306.
[25] A. Karlin, Curr. Opin. Neurobiol. 3 (1993) 299.
[26] M.L. Raves, M. Harel, Y.P. Pang, I. Silman, A.P. Kozikowski, J.L. Sussman, Nat. Struct. Biol. 4 (1997) 57.
[27] D.A. Stauffer, A. Karlin, Biochemistry 33 (1994) 6840.
[28] J.B. Mitchell, C.L. Nandi, I.K. McDonald, J.M. Thornton, S.L. Price, J. Mol. Biol. 239 (1994) 315.
[29] W. Zhong, J.P. Gallivan, Y. Zhang, L. Li, H.A. Lester, D.A. Dougherty, Proc. Natl. Acad. Sci. U.S.A. 95 (1998) 12088.
[30] O. Donini, D.F. Weaver, J. Comput. Chem. 19 (1998) 1515.
[31] O.M. Cabarcos, C.J. Weinheimer, J.M. Lisy, J. Chem. Phys. 110 (1999) 8429.
[32] R.L. Woodin, J.L. Beauchamp, J. Am. Chem. Soc. 100 (1978) 501.
[33] R.W. Taft, F. Anvia, J.-F. Gal, S. Walsh, M. Capon, M.C. Holmes, K. Hosn, G. Oloumi, R. Vasanwala, S. Yazdani, Pure Appl. Chem. 62 (1990) 17.
[34] B.C. Guo, J.W. Purnell, A.W. Castleman Jr., Chem. Phys. Lett. 168 (1990) 155.
[35] M.T. Rodgers, P.B. Armentrout, J. Phys. Chem. A 101 (1997) 1238.
[36] M.T. Rodgers, P.B. Armentrout, J. Phys. Chem. A 101 (1997) 2614.
[37] M.T. Rodgers, P.B. Armentrout, J. Phys. Chem. A 103 (1999) 4955.
[38] M.T. Rodgers, P.B. Armentrout, J. Chem. Phys. 109 (1998) 1787.
[39] M.T. Rodgers, K.M. Ervin, P.B. Armentrout, J. Chem. Phys. 106 (1997) 4499.
[40] M.T. Rodgers, P.B. Armentrout, Int. J. Mass Spectrom. 185–187 (1999) 359.
[41] R. Amunugama, M.T. Rodgers, Int. J. Mass Spectrom. 195/196 (2000) 439.
[42] M.T. Rodgers, P.B. Armentrout, J. Am. Chem. Soc. 122 (2000) 8548.
[43] M.T. Rodgers, J.R. Stanley, R. Amunugama, J. Am. Chem. Soc. 122 (2000) 10969.
[44] M.T. Rodgers, J. Phys. Chem. A 105 (2001) 2374.
[45] R. Amunugama, M.T. Rodgers, J. Phys. Chem. A 105 (2001) 9883.
[46] M.T. Rodgers, J. Phys. Chem. A 105 (2001) 8145.
[47] M.T. Rodgers, P.B. Armentrout, J. Am. Chem. Soc. 124 (2002) 2678.
[48] A.B. Valina, R. Amunugama, H. Huang, M.T. Rodgers, J. Phys. Chem. A 105 (2001) 11057.
[49] G. Vitale, A.B. Valina, H. Huang, R. Amunugama, M.T. Rodgers, J. Phys. Chem. A 105 (2001) 11351.
[50] R.C. Weast, M.J. Astle (Eds.), Handbook of Chemistry and Physics, CRC Press, Inc, Florida, 1982, p. E-61.
[51] K.J. Miller, J. Am. Chem. Soc. 112 (1990) 8533.
[52] (a) E. Teloy, D. Gerlich, Chem. Phys. 4 (1974) 417;
(b) D. Gerlich, Diplomarbeit, University of Freiburg, Federal Republic of Germany, 1971;
(c) D. Gerlich, in: C.-Y. Ng, M. Baer (Eds.), Advances in Chemical Physics Series, Wiley, New York, vol. 82, 1992, p. 1.
[53] N.F. Dalleska, K. Honma, P.B. Armentrout, J. Am. Chem. Soc. 115 (1993) 12125.
[54] N. Aristov, P.B. Armentrout, J. Phys. Chem. 90 (1986) 5135.
[55] D.A. Hales, P.B. Armentrout, J. Cluster Sci. 1 (1990) 127.
[56] K.M. Ervin, P.B. Armentrout, J. Chem. Phys. 83 (1985) 166.
[57] N.F. Dalleska, K. Honma, L.S. Sunderlin, P.B. Armentrout, J. Am. Chem. Soc. 116 (1994) 3519.
[58] (a) T.S. Beyer, D.F. Swinehart, Comm. Assoc. Comput. Machines 16 (1973) 379;
(b) S.E. Stein, B.S. Rabinovitch, J. Chem. Phys. 58 (1973) 2438;
(c) S.E. Stein, B.S. Rabinovitch, Chem. Phys. Lett. 49 (1977) 1883.
[59] J.A. Pople, H.B. Schlegel, K. Ragavachari, D.J. DeFrees, J.F. Binkley, M.J. Frisch, R.F. Whitesides, R.F. Hout, W.J. Hehre, Int. J. Quant. Chem. Symp. 15 (1981) 269;
D.J. DeFrees, A.D. McLean, J. Chem. Phys. 82 (1985) 333.
[60] F.A. Khan, D.C. Clemmer, R.H. Schultz, P.B. Armentrout, J. Phys. Chem. 97 (1993) 7978.
[61] E.V. Waage, B.S. Rabinovitch, Chem. Rev. 70 (1970) 377.
[62] W.J. Chesnavich, M.T. Bowers, J. Phys. Chem. 83 (1979) 900.
[63] M.B. More, E.D. Glendening, P.B. Armentrout, J. Phys. Chem. 100 (1996) 1605.
[64] D. Ray, D. Feller, M.B. More, E.D. Glendening, P.B. Armentrout, J. Phys. Chem. 100 (1996) 16116.
[65] F. Meyer, F.A. Khan, P.B. Armentrout, J. Am. Chem. Soc. 117 (1995) 9740.
[66] P.B. Armentrout, J. Simons, J. Am. Chem. Soc. 114 (1992) 8627.
[67] M.J. Frisch, G.W. Trucks, H.B. Schlegel, G.E. Scuseria, M.A. Robb, J.R. Cheeseman, V.G. Zakrzewski, J.A. Montgomery Jr., R.E. Stratmann, J.C. Burant, S. Dapprich, J.M. Millam, A.D. Daniels, K.N. Kudin, M.C. Strain, O. Farkas, J. Tomasi, V. Barone, M. Cossi, R. Cammi, B. Mennucci, C. Pomelli, C. Adamo, S. Clifford, J. Ochterski, G.A. Petersson, P.Y. Ayala, Q. Cui, K. Morokuma, D.K. Malick, A.D. Rabuck, K. Raghavachari, J.B. Foresman, J. Cioslowski, J.V. Ortiz, B.B. Stefanov, G. Liu, A. Liashenko, P. Piskorz, I. Komaromi, R. Gomperts, R.L. Martin, D.J. Fox, T. Keith, M.A. Al-Laham, C.Y. Peng, A. Nanayakkara, C. Gonzalez, M. Challacombe, P.M.W. Gill, B. Johnson, W. Chen, M.W. Wong, J.L. Andres, C. Gonzales, M. Head-Gordon, E.S. Replogle, J.A. Pople, Gaussian 98, Revision A.9, Gaussian, Inc., Pittsburgh, PA, 1998.
[68] A.D. Becke, J. Chem. Phys. 98 (1993) 5648.

[69] C. Lee, W. Yang, R.G. Parr, Phys. Rev. B 37 (1988) 785.
[70] The Hay–Wadt valence basis sets and effective core potentials were obtained from the Extensible Computational Chemistry Environment Basis Set Database (available on the Internet at http://www.emsl.pnl.gov:2080/forms/basisform.html), as developed and distributed by the Molecular Science Computing Facility, Environmental and Molecular Sciences Laboratory, which is part of the Pacific Northwest National Laboratory, P.O. Box 999, Richland, WA 99352, and funded by the U.S. Department of Energy. For the original valence basis set and ECP reference, see: P.J. Hay, W.R. Wadt, J. Chem. Phys. 82 (1985) 299.
[71] E.D. Glendening, D. Feller, M.A. Thompson, J. Am. Chem. Soc. 116 (1994) 10657.
[72] D. Walter, P.B. Armentrout, J. Am. Chem. Soc. 120 (1998) 3176.
[73] J.B. Foresman, ´Æ. Frisch, Exploring Chemistry with Electronic Structure Methods, 2nd ed., Gaussian, Pittsburgh, 1996, p. 64.
[74] S.F. Boys, R. Bernardi, Mol. Phys. 19 (1979) 553.
[75] F.B. Van Duijneveldt, J.G.C.N. van Duijneveldt-van de Rijt, J.H. van Lenthe, Chem. Rev. 94 (1994) 1873.
[76] I. Dzidic, P. Kebarle, J. Phys. Chem. 74 (1970) 1466.
[77] W.R. Davidson, P. Kebarle, J. Am. Chem. Soc. 98 (1976) 6125.
[78] N.F. Dalleska, B.L. Tjelta, P.B. Armentrout, J. Phys. Chem. 98 (1994) 4191.
[79] D. Feller, E.D. Glendening, R.A. Kendall, K.A. Peterson, J. Chem. Phys. 100 (1994) 49881.
[80] M.B. More, E.D. Glendening, D. Ray, D. Feller, P.B. Armentrout, J. Phys. Chem. 100 (1996) 1605.
[81] M.B. More, D. Ray, P.B. Armentrout, J. Phys. Chem. A 101 (1997) 1238.
[82] M.B. More, D. Ray, P.B. Armentrout, J. Phys. Chem. A. 101 (1997) 4254.
[83] M.B. More, D. Ray, P.B. Armentrout, J. Phys. Chem. A. 101 (1997) 7007.
[84] C. Lifshitz, Adv. Mass Spectrom. 11 (1989) 113.
[85] R.G. Wilson, G.R. Brewer, Ion Beams: With Applications to Ion Implantation, Wiley, New York, 1973, pp. 118–124.
[86] J.H. Williams, Acc. Chem. Res. 26 (1993) 593.